Coordination Chemistry Reviews 255 (2011) 451–458

Contents lists available at ScienceDirect

Coordination Chemistry Reviews

journal homepage: www.elsevier.com/locate/ccr

Review

# Mixed-metal one-dimensional sulfides—A class of materials with differences and similarities to oxides

Mark R. Harrison, M. Grazia Francesconi*

*Department of Chemistry, University of Hull, Cottingham Road, Hull HU6 7RX, United Kingdom*

**Contents**



ARTICLE INFO

*Article history:*
Received 28 July 2010
Accepted 4 October 2010
Available online 11 October 2010

*Keywords:*
Sulfides
One-dimensional structures
Transition metals

ABSTRACT

The higher degree of covalency in the metal–sulfide bond in sulfides compared to the metal–oxide bond in oxides often leads to the breakdown of the ionic model for the description of sulfides, making the two classes of materials rather dissimilar. This feature considers how one-dimensional ternary (or mixed-metal) sulfides can be considered a class of materials for which the ionic model is still valid. A selection of one-dimensional mixed-metal sulfides is described with the aim of highlighting some similarities and differences with oxides, especially oxides of the same stoichiometry.



## 1. Introduction

Sulfides are a large class of solid compounds, which, even though less studied than oxides, constantly attract interest from the scientific community due to their interesting, sometimes unique, structural and physical properties. Oxygen and sulfur both belong to group 6 with oxygen in the first row and sulphur in the second. Oxygen, as the anion $O^{2-}$ forms oxides with most metals and sulfur, as the $S^{2-}$ anion, forms sulfides. Sulfides of the electropositive metals, such as alkali and alkaline earth metals, show a large degree of ionic character and tend to adopt the same structure as oxides of the same stoichiometry. Sulfides of transition metals often show a prevalence of covalent or metallic character and their structures tend to differ from those of the corresponding oxides. Oxides tend to show structural similarities with fluorides, whereas sulfides tend to resemble halides further down in the group, as exemplified by the structural similarity of $TiO_2$ and $MnF_2$, showing the rutile structure and $TiS_2$ and $MnI_2$, showing the $CdI_2$ layered structure.

Monoxides and monosulfides, of transition metals in particular, show well how structures tend to differ between oxides and sulfides. All monoxides crystallise in the rock salt structure. Among the monosulfides, only MnS shows this structure, with others adopting mainly the NiAs structure, often with distortions and variations. Comparison between monoxides and monosulfides also illustrates the similarities and differences in bonding and electronic behaviour. The larger covalency of the $S^{2-}$ anion compared to the

* Corresponding author. Tel.: +44 1482465420; fax: +44 1482466410.
*E-mail address:* m.g.francesconi@hull.ac.uk (M.G. Francesconi).

0010-8545/$ – see front matter © 2010 Elsevier B.V. All rights reserved.
doi:10.1016/j.ccr.2010.10.008

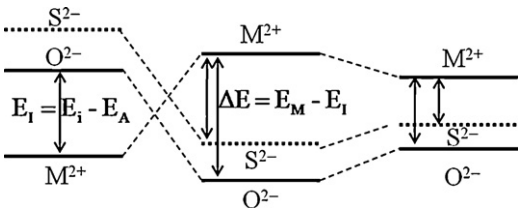


**Fig. 1.** Schematic general energy diagram for transition metal monoxides and monosulfides.

$O^{2-}$ anion leads to a smaller energy gap between the metallic and sulfide $3p^6$ levels than the metallic and oxide $2p^6$ levels. In fact, a simplified energy diagram of a transition metal monoxide can be built starting from the isolated ions, as shown in Fig. 1, with their relative energies, the ionisation potential ($E_i$) and the electron affinity ($E_A < 0$) [1].

When the anion and cation are arranged in a crystal lattice the strong electrostatic potential imposed by the surrounding ions, the Madelung energy ($E_M$), needs to be taken into account and the energy gap becomes $E_M - E_I$. For $(E_M - E_I) > 0$ an inversion of the $M^{2+}$ and $O^{2-}$ energies occurs. The gap between the $M^{2+}$ and $O^{2-}$ energies is then reduced by a degree of transfer of electrons from the anion to the cation, which reduces the effective ionic charge and, consequently, $E_M$. The electron affinity for sulfide anions is more negative than that of oxides, and this implies an increased value of $E_I$ and, consequentially, a reduced value of the separation $E_M - E_I$. One of the consequences of this reduced gap is that, for transition metals M = Mn–Zn, the energy of the trivalent $d^{n+1}$ cation may fall below the top energy of the sulphur bands, causing the creation of holes in these 3p bands, which makes higher oxidation states for the metal inaccessible and favours the formation of $(S_2)^{2-}$ anions. In fact, where the oxidation of MnO to $MnO_2$ implies the oxidation of manganese from 2+ to 4+, the oxidation of MnS to $MnS_2$ results in the oxidation of $S^{2-}$ to $(S_2)^{2-}$ with manganese maintaining the 2+ oxidation state [2]. In this way, the stronger covalent character of the metal–sulfide bond leads to more frequent breakdowns of the ionic model for sulfides than for oxides.

However, for a number of ternary or mixed-metal sulfides the ionic model still represents a good starting point for the description of the structure and properties. These ternary sulfides usually contain transition metals and electropositive elements (alkaline or alkaline earth metals) and it is the presence of the electropositive metal that, often, gives the transition metals oxidation states typical of salt-like compounds. It was first observed by Zintl that solid compounds, which contain both elements on the borderline between metals and non-metals and electropositive metals, contain certain characteristic structural units. These structural units can show structural similarities with units containing atoms of a different nature. For example the network of $[Si_4^{4-}]$ tetrahedra in NaSi is related to the tetrahedra network in white phosphorous. The Zintl concept has been extended to rationalise the structures of a number of ternary sulfides of general formula $A_xM_yS_z$ in which A is an electropositive metal and M a transition metal [3,4]. According to this model, sulfides can still be considered, to a certain extent, 'ionic compounds' in which the 'anion' is the $[M_xS_z]^{n-}$, gaining electrons from the metal A to give the cation $A^{n+}$. Interestingly, if sulfur is replaced by a halogen, X, giving rise to the $[M_xX_z]^{(n-z)}$ anion, these two structural units in some cases exhibit a close relationship, as observed for $[CoS_4]^{6-}$ units, related to $[CoCl_4]^{2-}$ units and $[PdS_2]^{2-}$ units related to $PdCl_2$ units. Also, the $[FeS_2]^{-}$ units show isostructurality with the $[MnS_2]^{2-}$ units, when $Fe^{3+}$ is replaced by the isoelectronic $Mn^{2+}$.

The validity of the ionic model as a starting point for the description of structural features in ternary sulfides is what allows chemists to apply similar reasoning to oxides and sulfides, such as charge neutrality, ionic size and Vegard's law within families of isostructural compounds, for example the $A_2MS_2$ (A = K, Rb, Cs; M = Mn, Co) series, in which the unit cell parameters increase with the increasing size of the alkali metal.

On the other hand, the combination of bonds of different nature, the more covalent M–S bond and the more ionic A–S bond, increases the tendency to form one- or two-dimensional structures and low dimensionality is much more commonly observed in sulfides than oxides. One-dimensional solids are of particular interest as they can be viewed as a link between molecular (polymer) and solid state chemistry, and can be described as a condensation of chains with strong intrachain bonding and weaker interchain bonding, often van der Waals forces [5]. Silvestre and Hoffmann highlighted this analogy when they investigated the band structure of one-dimensional sulfides such as $KPtS_2$ and $Na_2PdS_2$ by building up the electronic structure of the $(MS_2)_\infty$ chains from that of the dimer ($M_2S_6$) and considering a combination of crystal field (local) factors and longer range periodicity (inter unit cell) interactions [6].

Strong bonds within the chains and weak bonds between the chains not only favour a large degree of anisotropy in the structure, it also affects the physical properties, as exemplified by the many cases of $S^{2-}$ mediated magnetic interactions located along chains of $[M_xS_z]^{n-}$ polyhedra [7].

The sulfides under consideration in this feature are a selection of some families of one-dimensional ternary sulfides of general formula $A_xM_yS_z$, where A = electropositive metal and M = transition metal (groups 4–12) and A and M occupy different crystallographic sites. Structural features and physical properties reported in the literature will be summarised and, where possible, structural similarities with other classes of compounds will be included. Rare earth transition metal sulfides are not considered here as they are included in an extensive review published in 2002 [8]. Furthermore, sulfides not belonging to families such as $K_2Ta_2S_{10}$ [9], $Ba_{1-x}Fe_2S_4$ [10], $Na_3Cu_4S_4$ [11], $Ba_3CrS_5$ [12], $Ba_3Cr_2S_6$ [12], $Tl_2TiS_4$ [13], $Na_5Co_2S_5$ [14], $Ba_7Fe_6S_{14}$ [15] and $Ba_6Fe_8S_{15}$ [16] will not be discussed here.

It is worth noticing that alkali metals outnumber largely alkaline earth metals as "counter cations" in one-dimensional sulfides and that the only alkaline earth metal found in one-dimensional sulfides seems to be barium, with the exception of the compound $SrZrS_3$ [17,18]. The families of one-dimensional ternary sulfides described here are, first, broadly divided in two groups, 'sulfides containing alkali metals' and 'sulfides containing barium'. A further subdivision is based on the stoichiometries, which are listed in order of decreasing $n/x$ ratio. The Zintl–Klemm concept states that the connectivity of the building units within the $[M_xS_z]^{n-}$ structural entities increases with decreasing of the $n/x$ ratio. This has been extended by Bronger and Müller to the analysis of the connectivities between M–S polyhedra in alkali metal containing one-dimensional ternary sulfides exemplified by the comparison between $AFe_2S_3$ and $AFeS_2$. $AFe_2S_3$ shows chains of double Fe–S tetrahedral [19] whereas $AFeS_2$, which has a higher alkali metal to iron ratio, contains chains of single tetrahedral [20]. In general a higher alkali metal stoichiometry forces a higher sulfide stoichiometry, increasing the number of linking points between the metal polyhedra and reducing the cross linking [21].

## 2. Ternary one-dimensional sulfides $A_xM_yS_z$ with A = alkaline metal

### 2.1. $A_2MS_2$ (A = K, Rb, Cs; M = Mn, Co)

These compounds are isostructural with $K_2ZnO_2$ [22] and, therefore, provide a good example of similarity between oxides and one-dimensional sulfides. Their structure includes chains of edge

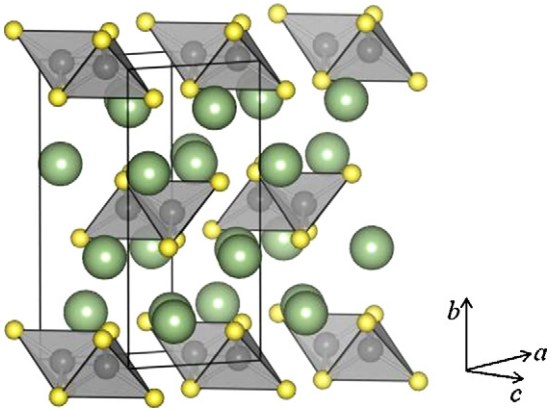


**Fig. 2.** Structure of $A_2MS_2$. The gray polyhedra represent $MS_4$ tetrahedra with yellow sulfur at the vertices and A cations represented by light green spheres. [23].

**Table 1a**
Unit cell parameters of the sulfides belonging to the $A_2CoS_2$ family (A = Na, K, Rb, Cs).

| $A_2CoS_2$ | $Na_2CoS_2$ | $K_2CoS_2$ | $Rb_2CoS_2$ | $Cs_2CoS_2$ |
|---|---|---|---|---|
| *a* (Å) | 6.373(3) | 6.710(2) | 6.959(1) | 7.232(5) |
| *b* (Å) | 11.208(4) | 12.491(5) | 13.096(2) | 13.722(7) |
| *c* (Å) | 5.850(2) | 6.085(2) | 6.219(1) | 6.322(4) |
| *V* (Å$^3$) | 417.86 | 510.01 | 566.77 | 627.38 |

**Table 1b**
Unit cell parameters of the sulfides belonging to the $A_2MnS_2$ family (A = K, Rb, Cs) [23].

| $A_2MnS_2$ | $K_2MnS_2$ | $Rb_2MnS_2$ | $Cs_2MnS_2$ |
|---|---|---|---|
| *a* (Å) | 6.932(2) | 7.119(1) | 7.589(2) |
| *b* (Å) | 12.62(3) | 13.140(2) | 13.781(4) |
| *c* (Å) | 6.179(2) | 6.295(1) | 6.414(3) |
| *V* (Å$^3$) | 541.24 | 588.86 | 670.8 |

sharing $MS_4$ tetrahedra along the *c* axis (Fig. 2). The unit cell parameters are shown in Tables 1a and 1b and exhibit an increase with increasing ionic radius of the alkali metal, supporting the argument that the ionic model is applicable to one-dimensional sulfides.

The magnetic properties of the members of the $A_2MnS_2$ family have been characterised and suggest antiferromagnetic interactions between the Mn atoms within the chains [23].

$K_2CoS_2$ has been analysed by neutron diffraction along with magnetic susceptibility and showed antiferromagnetic coupling of the cobalt ions along the chains with an onset of 3D order at 9.5 K.

**Table 2**
Unit cell parameters of the sulfides belonging to the $A_2MS_2$ family (A = Na, K, Rb, M = Pt, Pd). Errors for $K_2PtS_2$ and $Rb_2PtS_2$ were not reported.

| $A_2PtS_2$ | $K_2PtS_2$ [24] | $Rb_2PtS_2$ [24] | $Na_2PtS_2$ [25] | $Na_2PdS_2$ [25] |
|---|---|---|---|---|
| *a* (Å) | 9.37 | 9.87 | 3.548(1) | 3.539(2) |
| *b* (Å) | 7.08 | 7.33 | 10.437(1) | 10.411(4) |
| *c* (Å) | 3.59 | 3.64 | 10.877(2) | 10.886(4) |
| *V* (Å$^3$) | 238.16 | 263.34 | 402.78 | 401.09 |

### 2.2. $A_2MS_2$ (A = Na, K, Rb, M = Pt, Pd)

These compounds all show square planar coordination of the sulfur around the Pt/Pd atoms with the square planes edge-connected in chains running along the short axis. The compounds $K_2PtS_2$ and $Rb_2PtS_2$ crystallise in the space group *Immm* and the square planes are parallel to the *c* axis (Fig. 3a) [24]. The compounds $Na_2PtS_2$ and $Na_2PdS_2$ are slightly different as the square planes are tilted with respect to the short axis, *a*, (Fig. 3b) and crystallise in the space group $Cmc2_1$. The unit cell parameters are shown in Table 2 [25].

A theoretical study, using density functional methods, has been undertaken on $PtS_2$ chain compounds and correctly predicted the structure of $K_2PtS_2$ and its semiconductive one-dimensional behaviour, provided long range Coulomb interactions were considered [26].

### 2.3. $A_2TiS_3$ (A = Cs, K)

These two compounds are structurally very similar and consist of chains of $TiS_5$ square pyramids linked by edges with the apices of alternate pyramids pointing in opposite directions (Fig. 4). The difference between the two structures is a slight monoclinic distortion from the $Cs_2TiS_3$ to the $K_2TiS_3$ structure. The unit cell parameters for $K_2TiS_3$ are; $a = 11.667(6)$ Å, $b = 8.325(4)$ Å, $c = 6.494(4)$ Å and $\beta = 91.81(4)^\circ$ (*C*2/*c*). The unit cell parameters for $Cs_2TiS_3$ are $a = 12.51(8)$ Å, $b = 9.03(6)$ Å and $c = 6.55(0)$ Å (*Cmc*2/1) [27,28]. There is also a small but significant difference in the apical Ti–S distances, as $K_2TiS_3$ shows Ti–S = 2.188(3) Å and $Cs_2TiS_3$ has Ti–S = 2.23(2) Å [27].

### 2.4. $A_3Fe_2S_4$ (A = Na, K, Rb, Cs, Tl)

These compounds crystallise in the orthorhombic space group *Pnma* and contain one-dimensional zigzagging chains of edge-linked distorted $FeS_4$ tetrahedra (Fig. 5) [29]. The compounds are isotypic except $Cs_3Fe_2S_4$, in which the Fe–Fe–Fe bond angle (175.3°) is considerably higher than the others (160°) and Cs shows

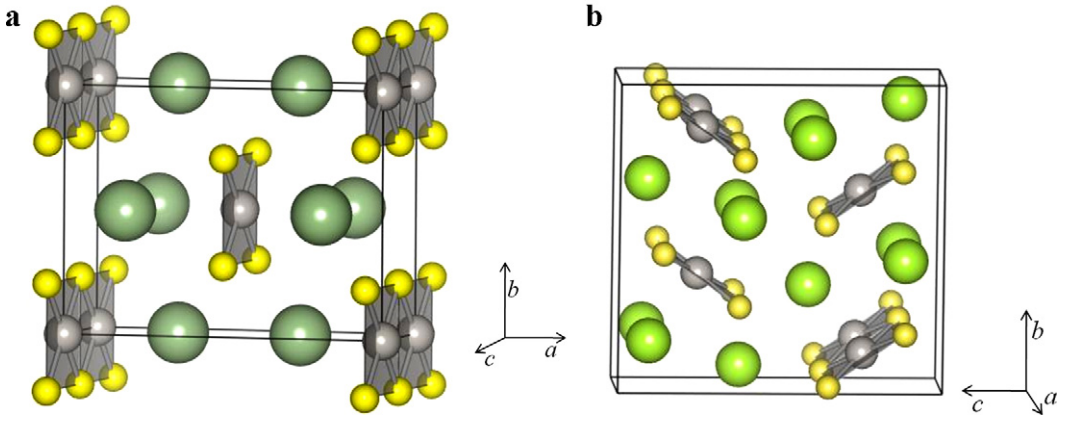


**Fig. 3.** Representation of (a) $A_2PtS_2$ (A = K, Rb) [24] and (b) $Na_2MS_2$ (M = Pt, Pd) structure [25], showing edge sharing square planes of silver M atoms and yellow sulfur atoms with green A atoms in chains in between.

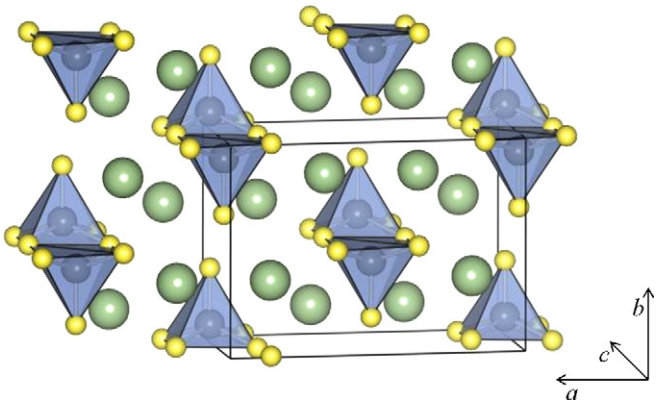


**Fig. 4.** Structure of $K_2TiS_3$ [27]. The blue polyhedral are $TiS_5$ square pyramids with yellow sulfur at the vertices. The green spheres are K cations.

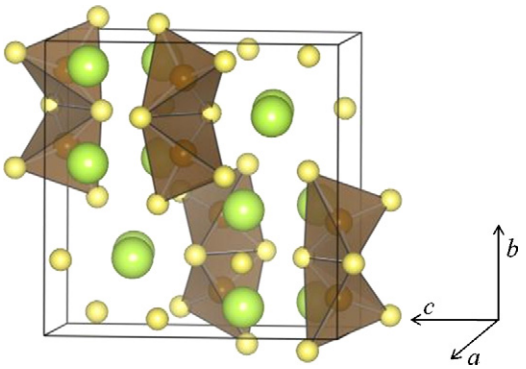


**Fig. 5.** Structure of $A_3Fe_2S_4$ (A = Na, K, Rb, Tl) [29]. The brown tetrahedra are $FeS_4$ with yellow sulfur at the vertices. The green spheres are A atoms.

a different co-ordination. The lattice parameters are shown in Table 3.

In $Na_3Fe_2S_4$ the Fe atoms are coupled antiferromagnetically with a transition to 3D ferrimagnetism at 149 K. Mössbauer spectroscopy showed only one resonance between 4.2 K and 300 K, indicating that although iron is formally in a mixed valence state (+2/+3), delocalisation of electrons results in an averaging of the oxidation state over the iron atoms [31]. $Tl_3Fe_2S_4$ shows three-dimensional antiferromagnetic order with a Néel temperature $T_N = 90(5)$ K [32].

### 2.5. $AFeS_2$ (A = K, Rb, Cs, Tl)

These compounds show $FeS_4$ tetrahedra edge linked in one-dimensional chains with the alkali metal ions (or Tl) between these chains (Fig. 6).

The $[FeS_2]$ framework is related to the $SiS_2$ structure and the alkali metals between the chains are characterised by different coordination numbers according to their size. $KFeS_2$ and $RbFeS_2$ and $TlFeS_2$ are isostructural and both monoclinic (Fig. 6a) whilst $CsFeS_2$ is orthorhombic (Fig. 6b). Unit cell parameters and space groups for all the compounds in the $AFeS_2$ series are shown in Table 4.

The main difference between the monoclinic ($KFeS_2$ and $RbFeS_2$) and orthorhombic ($CsFeS_2$) structures is in the Fe–Fe distances. In both cases the interchain distances are around 7 Å and the tetrahedra are distorted with Fe–S distances ranging from 2.18 Å to 2.28 Å. However, in $KFeS_2$ the Fe–Fe intrachain distance is 2.7 Å whilst in $CsFeS_2$ the distance alternates between 2.61 Å and 2.82 Å. This difference influences the magnetic properties of the two compounds [36].

$KFeS_2$ and $RbFeS_2$ are both S = 1/2 one-dimensional antiferromagnets with a transition to three-dimensional antiferromagnetic order at 250 K and 188 K, respectively [20].

$CsFeS_2$ shows a broad maximum in susceptibility at around 800 K but is paramagnetic until a structural and magnetic phase transition at 70 K. The alternating intrachain Fe–Fe distances result in two intrachain exchange constants of $J = -640$ K for the short distance, and $J_2 = 192$ K for the longer distance, which average out to $T_c - 440$ K (the value for $KFeS_2$). $CsFeS_2$ and $KFeS_2$ can, however, be viewed as low and high temperature analogues of a spin-Peierls system as the bond lengths are varied in $CsFeS_2$ and regular in $KFeS_2$ with roughly the same average distance [36]. Interestingly, $TlFeS_2$ shows the alternating Fe–Fe intrachain distances of 2.617 Å and 2.703 Å as in $CsFeS_2$, but contains antiferromagnetic covalent chains with a switch to collinear 3D order at $T_N = 196(1)$ K with intrachain coupling constant $J = -55(3)$ meV [35].

**Table 3**
Unit cell parameters of the sulfides belonging to the $A_3Fe_2S_4$ family (A = Na, K, Rb, Cs, Tl). Errors for $Tl_3Fe_2S_4$ were not reported.

| $A_3Fe_2S_4$ | $Na_3Fe_2S_4$ [29] | $K_3Fe_2S_4$ [30] | $Rb_3Fe_2S_4$ [30] | $Cs_3Fe_2S_4$ [30] | $Tl_3Fe_2S_4$ [31] |
|---|---|---|---|---|---|
| $a$ (Å) | 6.6333(5) | 7.157(3) | 7.4069(7) | 7.540(2) | 7.38 |
| $b$ (Å) | 10.675(1) | 10.989(4) | 11.141(1) | 11.168(5) | 10.73 |
| $c$ (Å) | 10.677(2) | 11.560(4) | 11.997(1) | 12.923(4) | 11.14 |
| $V$ (Å$^3$) | 756.04 | 909.17 | 990 | 1088.2 | 882.15 |

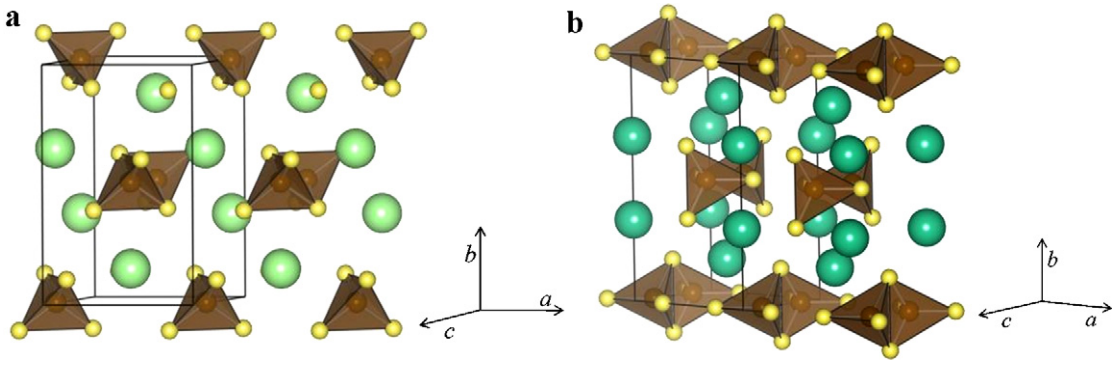


**Fig. 6.** Structure of (a) $AFeS_2$ and (b) $CsFeS_2$ with A = K, Rb, Tb [33,34]; the brown tetrahedra are $FeS_4$ with yellow sulfur at the vertices. The green spheres are A cations in (a) and Cs cations in (b).

**Table 4**
Unit cell parameters of the sulfides belonging to the $AFeS_2$ family family (A = K, Rb, Cs, Tl). Errors were not reported.

| $AFeS_2$ | $KFeS_2$ [33] | $RbFeS_2$ [33] | $CsFeS_2$ [34] | $TlFeS_2$ [35] |
|---|---|---|---|---|
| Space group | *C*2/*c* | *C*2/*c* | *Immm* | *C*2/*m* |
| *a* (Å) | 7.05 | 7.215 | 7.159 | 11.68 |
| *b* (Å) | 11.28 | 11.70 | 11.91 | 5.32 |
| *c* (Å) | 5.4 | 5.42 | 5.409 | 10.53 |
| *β* (°) | 112.5 | 112.0 | 90.0 | 144.6 |
| *V* (Å$^3$) | 396.97 | 426.38 | 460.64 | 379.03 |

**Table 5**
Unit cell parameters for the sulfides belonging to the $AFe_2S_3$ family (A = K, Rb, Cs, Ba).

| $AFe_2S_3$ | $KFe_2S_3$ [19] | $RbFe_2S_3$ [19] | $CsFe_2S_3$ [19] | $BaFe_2S_3$ [39] |
|---|---|---|---|---|
| *a* (Å) | 9.0415(13) | 9.2202(7) | 9.5193(8) | 8.7835(9) |
| *b* (Å) | 11.0298(17) | 11.2429(9) | 11.5826(10) | 11.219(1) |
| *c* (Å) | 5.4177(6) | 5.4450(3) | 5.4820(4) | 5.2860(5) |
| *V* (Å$^3$) | 540.29 | 564.44 | 604.44 | 520.89 |

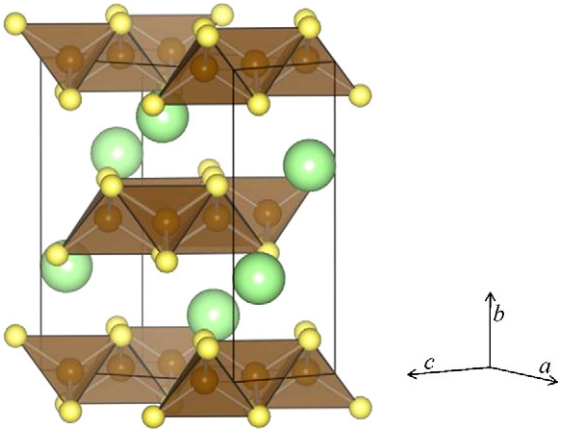


**Fig. 7.** Structure of $AFe_2S_3$ (A = K, Rb, Cs, Ba) [19]. The brown tetrahedra are $FeS_4$ with yellow sulfur at the vertices. The green spheres are A cations.

**Table 6**
Unit cell parameters and Debye temperatures for the solid solution $K_xBa_{1-x}Fe_2S_3$ ($0 \le x \le 0.3$) [40].

| *x* | *a* (Å) | *b* (Å) | *c* (Å) | *V* (Å$^3$) | *D* (K) |
|---|---|---|---|---|---|
| $K_xBa_{1-x}Fe_2S_3$ | | | | | |
| 0 | 8.795(2) | 11.228(3) | 5.285(2) | 521.895 | 435 |
| 0.05 | 8.790(2) | 11.216(3) | 5.294(5) | 521.928 | 418 |
| 0.1 | 8.808(2) | 11.193(3) | 5.305(1) | 523.009 | 427 |
| 0.3 | 8.824(4) | 11.171(5) | 5.323(2) | 524.704 | 405 |

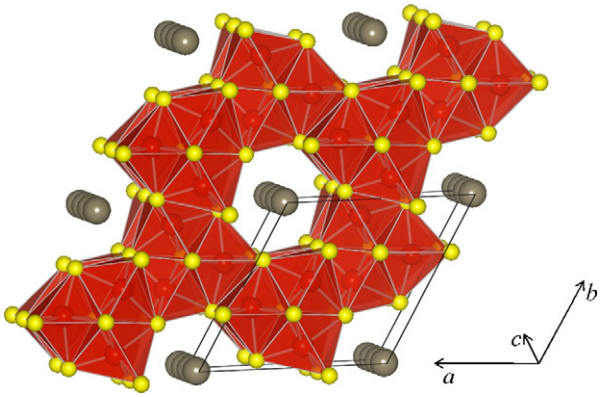


**Fig. 8.** Structure of $AV_6S_8$, showing hexagonal channels formed by red, linked $VS_8$ octahedra with yellow sulfur at the vertices and silver A cations in the channels [43]. The sulfur (yellow) and A (silver) cations are relatively small for clarity.

In all of these compounds iron is formally trivalent but also exhibits considerable delocalisation due to short Fe–Fe bonds. For example, $KFeS_2$ can be described as containing $Fe^{3+}$ ($3d^4$) with one itinerant electron [20].

The solid solution $CsGa_{1-x}Fe_xS_2$ forms a single monoclinic phase with values of $x \le 0.25$ and an orthorhombic phase for $x \ge 0.95$ [37]. Interestingly, susceptibility, Mössbauer and neutron diffraction data indicate low-spin configuration for the iron cation, a rather unusual situation for $Fe^{3+}$ in a tetrahedral environment.

### 2.6. $AFe_2S_3$ (A = K, Rb, Cs, Ba)

These compounds are all orthorhombic *Cmcm* (unit cell parameters listed in Table 5) and consist of chains of double tetrahedra running along the *c* axis (Fig. 7). Mössbauer, resistivity and susceptibility measurements have been used to determine the oxidation state of iron in $BaFe_2S_3$. The single quadrupole shift, low resistivity (~0.5 Ωcm) and magnetic moment of 4.85 μB all point to significant delocalisation of one half electron per cation [38]. In $KFe_2S_3$, iron is formally in oxidation state +2.5 with a random distribution of $Fe^{2+}$ and $Fe^{3+}$ over the single iron crystallographic site [39].

A solid solution of $K_xBa_{1-x}Fe_2S_3$ exists with *a* and *b* values increasing and *c* decreasing with increasing values of *x* (Table 6) [40].

### 2.7. $AV_6S_8$ (A = Na, K, Rb, Cs, In, Tl)

Crystallising in the hexagonal space group $P6_3$ the main structural feature of these compounds are the interpenetrating edge and face sharing $VS_6$ octahedra resulting in hexagonal channels filled with A atoms (Fig. 8). The V atoms are also linked in zigzagging chains with an average V–V distances of 2.86 Å, comparable to the distance in metallic vanadium (2.61 Å) [41].

The unit cell parameters of the $AV_6S_8$ compounds are shown in Table 7. It can be seen that the value of *a* increases with increasing ionic radius of the A cation whilst the *c* axis, which is the direction of the channels, changes only slightly [42]. These isotypic compounds are all superconductive (except for

**Table 7**
Unit cell parameters and $T_c$ for compounds in the series $AV_6S_8$ (A = Na, K, Rb, Cs, Tl, In). Errors for $InV_6S_8$ and $TlV_6S_8$ were not reported.

| $AV_6S_8$ | $NaV_6S_8$ [43] | $InV_6S_8$ [44] | $KV_6S_8$ [43] | $TlV_6S_8$ [42] | $RbV_6S_8$ [43] | $CsV_6S_8$ [43] |
|---|---|---|---|---|---|---|
| *a* (Å) | 9.1552(1) | 9.1711 | 9.1897(1) | 9.20400 | 9.2125(1) | 9.2572(1) |
| *c* (Å) | 3.3087(31) | 3.2972 | 3.2800(19) | 3.30580 | 3.3075(20) | 3.2847(14) |
| *V* (Å$^3$) | 240.1727 | 240.1700 | 239.8872 | 242.5272 | 243.1003 | 243.7730 |

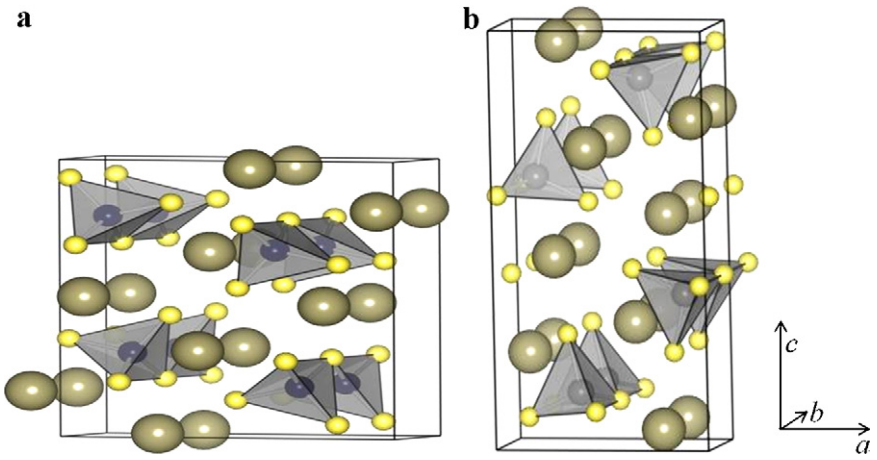


**Fig. 9.** Structure of the compounds $Ba_2MS_3$ where (a) M = Fe, Co, Zn and (b) M = Mn, Hg, Cd [52,46]. The gray tetrahedra are $MS_4$ with yellow sulfur at the vertices. The green spheres are Ba cations.

**Table 8**
Unit cell parameters of the sulfides belonging to the $Ba_2MS_3$ family (M = Mn, Hg, Cd, and Fe, Co, Zn). Standard deviations for $Ba_2ZnS_3$ were not reported.

| $Ba_2MS_3$ | $Ba_2MnS_3$ [46] | $Ba_2CdS_3$ [47] | $Ba_2HgS_3$ [48] | $Ba_2FeS_3$ [16] | $Ba_2CoS_3$ [49] | $Ba_2ZnS_3$ [50] |
|---|---|---|---|---|---|---|
| $a$ (Å) | 8.814(5) | 8.9145(6) | 8.93(1) | 12.087(5) | 12.000(1) | 12.05 |
| $b$ (Å) | 4.302(2) | 4.3356(2) | 4.35(7) | 4.246(2) | 4.205(2) | 4.21 |
| $c$ (Å) | 17.048(8) | 17.2439(9) | 17.25(7) | 12.359(5) | 12.470(1) | 12.65 |
| $V$ (Å$^3$) | 646.42 | 666.47 | 671.51 | 634.28 | 628.42 | 641.74 |

$NaV_6S_8$) with the $T_c$ for the stoichiometric compounds shown in Table 7.

These compounds can also show non-integer stoichiometric indices such as $A_xV_6S_8$ ($x < 1$) with the structure remaining stable for $x \geq 0.2$. Many of these non-stoichiometric compounds are also superconductive. $Tl_xV_6S_8$, has critical temperatures $T_c = 3.5$ K for $x = 0.61$ and $T_c = 0.74$ K for $x = 0.26$. $In_xV_6S_8$ is superconductive at $T_c = 0.95$ K for $x = 0.63$ and at $T_c < 0.02$ K for $x = 0.46$ [41].

## 3. Ternary one-dimensional sulfides $A_xM_yS_z$ with A = alkaline-earth metal

### 3.1. $Ba_2MS_3$ (M = Mn, Hg, Cd, and Fe, Co, Zn)

Two families of structurally similar sulfides show the 213 stoichiometry: $Ba_2MS_3$ with M = Mn, Hg, Cd and $Ba_2MS_3$ with M = Fe, Co, Zn. Both $Ba_2MS_3$ families show one-dimensional chains of corner linked M–S tetrahedral interleaved by $Ba^{2+}$ cations and two crystallographically different sites for $Ba^{2+}$ (Fig. 9). However, $Ba_2MS_3$ (M = Fe, Co, Zn) show the $K_2CuCl_3$-type structure, while

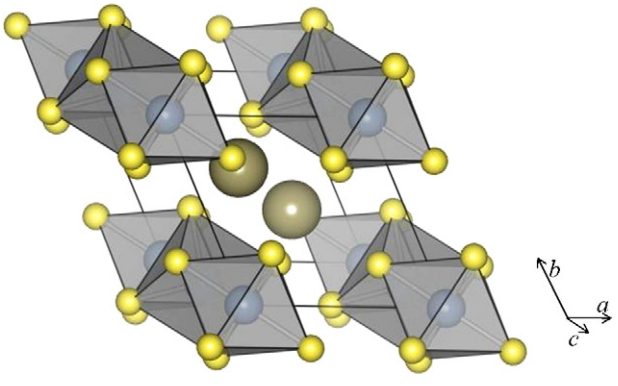


**Fig. 10.** Structure of $BaMS_3$ [56]; the gray polyhedra represent the M–S octahedra with yellow sulfur at the vertices and the green spheres represent Ba cations.

**Table 9**
Unit cell parameters of the sulfides belonging to the $BaMS_3$ family (M = Ti, V, Nb, Ta).

| $BaMS_3$ | $BaTiS_3$ [56] | $BaVS_3$ [57] | $BaNb_{0.98}S_3$ [58] | $BaTaS_3$ [59] |
|---|---|---|---|---|
| $a$ (Å) | 6.756(1) | 6.7283(5) | 6.840(2) | 6.846(5) |
| $c$ (Å) | 5.798(1) | 5.6263(5) | 5.745(2) | 5.744(5) |
| $V$ (Å$^3$) | 229.19 | 219.14 | 232.77 | 233.14 |

$Ba_2MS_3$ (M = Mn, Hg, Cd) show the $K_2AgI_3$-type structure. Shoemaker reported that the differences between the $K_2CuCl_3$ and $K_2AgI_3$ structures lie in the connectivity of the K–(Cl/I) polyhedra (or the Ba–S polyhedra of $Ba_2MS_3$) with the $Ba^{2+}$ polyhedra forming chains in $Ba_2MnS_3$ and dimeric units in $Ba_2CoS_3$ [45]. The unit cell parameters of the compounds in both groups are shown in Table 8.

An investigation into the magnetic susceptibilities of $Ba_2FeS_3$, $Ba_2CoS_3$ and $Ba_2MnS_3$ showed features consistent with quasi-one-dimensional antiferromagnetic short-range ordering [51]. Intrachain interactions, $J$, of −20, −15 and −12 K (in good agreement with value of −12.3(5) K previously reported for $Ba_2MnS_3$ and $Ba_2MnSe_3$) [46] were found for $Ba_2FeS_3$, $Ba_2CoS_3$ and $Ba_2MnS_3$. Long range magnetic ordering was found for all three compounds at 4.2 K due to interchain interactions [51]. The magnetic susceptibility of $Ba_2CoS_3$ has been reinvestigated and the data again showed a broad peak indicative of one-dimensional magnetic ordering but also a transition to long range order, at 46 K [49,52].

$Ba_2MnS_3$ is insulating with a room temperature resistivity of $10^2$–$10^3\,\Omega$ cm [53]. The resistivity of $Ba_2CoS_3$ is much lower at $\sim 10^{-1}\,\Omega$ cm and thermopower measurements were indicative of metallic like conduction [54]. An investigation into $Ba_2FeS_3$ suggests limited electron delocalisation. The high resistivity ($10^4\,\Omega$ cm), the effective magnetic moment of 5.29 $\mu_B$ and Mössbauer spectroscopy suggest that iron is present as $Fe^{2+}$ [38].

Interestingly, $Ba_2CoS_3$ shows negative magnetoresistance approximately −1.7% in a 7 T field at 10 K which is higher than that of the only other one dimensional sulfide so far reported to show negative MR [54]. Recently, it was reported that this negative magnetoresistance can be increased up to 9% via partial isovalent substitution of $Co^{2+}$ with the diamagnetic $Zn^{2+}$ [55].

**Table 10**
List of selected structural features for the families of sulfides described in this review.

| Family of one-dimensional sulfides $A^+[M_xS_z]^{n-}$ | Coordination of the transition metal (M) | Connectivity of coordination polyhedra within $[M_xS_z]^{n-}$ | $n/x$ ratio |
|---|---|---|---|
| *One-dimensional sulfides with A = alkaline metal* | | | |
| $A_2MS_2$ | Tetrahedral | Edge | 2 |
| $A_2MS_2$ M = Pd, Pt | Square planar | Edge | 2 |
| $A_2TiS_3$ | Pyramidal | Edge | 2 |
| $A_3Fe_2S_4$ | Tetrahedral | Edge | 3/2 |
| $AFeS_2$ | Tetrahedral | Edge | 1 |
| $AFe_2S_3$ | Tetrahedral (double) | Edge | 1/2 |
| $AV_6S_8$ | Octahedral | Face | 1/6 |
| *One-dimensional sulfides with A = alkaline-earth metal* | | | |
| $Ba_2MS_3$ | Tetrahedral | Corner | 4 |
| $BaMS_3$ | Octahedral | Face | 2 |

### 3.2. $BaMS_3$ (M = Ti, V, Nb, Ta)

The structure of this family of sulfides consists of face linked $MS_6$ octahedra running in chains along the *c* axis (Fig. 10). The space group of the $BaMS_3$ compounds is $P6_3/mmc$, the unit cell parameters are shown below in Table 9.

These ternary sulfides provide a not-so-common example of isostructurality with a ternary oxide, namely $BaNiO_3$, as well as to halides, namely $CsNiCl_3$ [60], and $CsCdBr_3$ [61]. These compounds provide a good example on the variation of physical properties as a function of the size or oxidation state of the cations as well as the effects of non-stoichiometry.

$BaTiS_3$, the only member of the series to contain a $d^0$ cation, $Ti^{4+}$, shows semiconducting properties. $BaVS_3$ is a metallic Pauli paramagnet and undergoes a transition to an antiferromagnetic semiconductor at 70 K with no associated structural (or spin-Peierls) transition. A slight structural distortion which induces some zigzagging of the chains does occur at 250 K [62]. A partial solid solution of $BaV_xTi_{1-x}S_3$ was also reported, with $BaV_{0.2}Ti_{0.8}S_3$ showing negative magnetoresistance of 0.7% at 80 K in a 6 T field [63,64].

$BaTaS_3$ is a metallic like conductor as the Ta-Ta distance, 2.872(2) Å, is small enough for some direct d-orbital overlap. The non-stoichiometric $BaTa_{0.8}S_3$ is semiconductive and diamagnetic. There is no ordering of the Ta vacancies and the tantalum oxidises partially to $Ta^{5+}$ to counterbalance the reduction in positive charge.

The properties of '$BaNbS_3$' are in doubt due to difficulties in confirming the correct stoichiometry and the sensitivity of the properties to this stoichiometry. $BaNbS_3$ was initially reported as diamagnetic and semiconducting but later studies suggested that the composition of that sample was $BaNb_{0.8}S_3$ [65]. Other groups have reported diamagnetism and a metal-to-semiconductor transition at 620 K due to the formation of Nb–Nb dimers [66]. Others have suggested that the stoichiometric $BaNbS_3$ shows metallic conductivity, whilst the sulfur deficient compound $BaNbS_{3-\delta}$ undergoes a semiconductor–metal transition (at 130 K for $BaNbS_{2.89}$) [67]. The most recent work suggests that with non-stoichiometry of sulfur, $BaNbS_{3+\delta}$, a semiconductor-to-metal transition occurs between 146 and 215 K for values of $2.96 \geq 3+\delta \leq 3.06$ with temperature independent magnetic susceptibility [68].

Interestingly, $SrZrS_3$ (*Pnma*; $a = 8.5254(7)$ Å, $b = 3.8255(3)$ Å, $c = 13.9246(12)$ Å) adopt the $(NH_4)CdCl_3$ type structure, which consists of chains of edge sharing octahedra running along the *b* axis, at temperatures below 980 °C [17], as well as at high pressure (Fig. 11) [18].

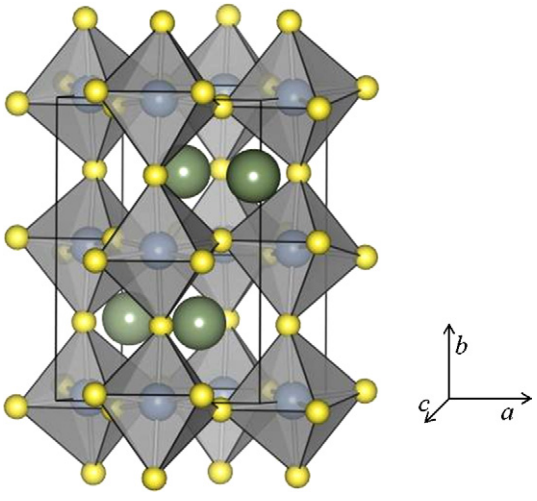


**Fig. 11.** Structure of $SrZrS_3$ [17]; the gray polyhedra are Zr–S octahedra, the green spheres represent Sr cations and the yellow spheres sulfur.

## 4. Conclusions

Some general trends can be seen within the families of one-dimensional sulfides discussed in this feature. Within the 'anions', $[M_xS_z]^{n-}$, the transition metals show a preference for the tetrahedral geometry and edge-connectivity, as it can be seen in the case of $AFeS_2$, $A_2CoS_2$ and $A_2MnS_2$, with their structure based on that of $SiS_2$ [69].

The list of values reported in Table 10 suggests that the edge-sharing connectivity of tetrahedra in $[M_xS_z]^{n-}$ is, broadly speaking, obtained for $1 \leq n/x < 4$, even though the data included are not sufficient to draw any definite conclusion and, certainly, other factors, such as electronic configuration and formal oxidation state of the metal will certainly play an important role. For example, in the $A_2MS_2$ family the transition metal shows tetrahedral coordination except in the case of palladium and platinum, known to prefer square planar configuration, which stabilises their $nd^8$ electronic configuration.

Sulfides showing edge- and face-sharing connectivity often show complex electronic properties, as the metal–sulphur and metal–metal distances are often of a similar length. This is caused by competition between superexchange interactions caused by the high degree of covalency in M–S bonds resulting in a large overlapping of metal and non-metal orbitals and the formation of d-bands resulting from short metal–metal distances allowing direct overlap of metal orbitals.

In conclusion, the main difference between sulfides and oxides relates to the greater covalency of the metal–anion bond in sulfides. However, one-dimensional ternary sulfides, though different, do show a degree of similarity with oxides. Oxides are the most studied compounds in solid state chemistry and it is therefore important to relate any class of materials to oxides to aid interpretation and even prediction of structure and properties of novel compounds.

## Acknowledgements

The authors thank the EPSRC for supporting this work (Grant EP/E029469).

## References

[1] J.B. GtLlenough, Some Comparisons of Flouride ides and Sulti,:s containing Divalent Transition Elements in: C.N.R. Rao (Ed.), Proc. Winter School in Solid State Chemistry IIT, Kanpur, India, December 1971. Marcel Dekkar, New York, 1993, p. 288.
[2] J.B. Goodenough, J. Alloy Compd. 262 (1997) 1.
[3] W. Bronger, P. Muller, J. Less Common Met. 100 (1984) 241.
[4] W. Bronger, Pure Appl. Chem. 57 (1985) 1363.
[5] J. Rouxel, Acc. Chem. Res. 25 (1992) 328.
[6] J. Silvestre, R. Hoffmann, Inorg. Chem. 24 (1985) 4108.
[7] W. Bronger, Angew. Chem., Int. Ed. Engl. 20 (1981) 52.
[8] K. Mitchell, J.A. Ibers, Chemical Reviews 102 (2002) 1929.
[9] Y.D. Wu, C. Nather, W. Bensch, J. Solid State Chem. 178 (2005) 1569.
[10] M. Onoda, K. Kato, Acta Crystallogr., Sect. B: Struct. Sci. 47 (1991) 630.
[11] C. Burschka, Z. Naturforsch, B: Chem. Sci. 34 (1979) 396.
[12] H. Fukuoka, Y. Miyaki, S. Yamanaka, J. Solid State Chem. 176 (2003) 206.
[13] K.O. Klepp, Z. Naturforsch., B: Chem. Sci. 40 (1985) 229.
[14] K.O. Klepp, W. Bronger, J. Less Common Met. 98 (1984) 165.
[15] I.E. Grey, H. Hong, H. Steinfink, Inorg. Chem. 10 (1971) 340.
[16] H.Y. Hong, H. Steinfink, J. Solid State Chem. 5 (1972) 93.
[17] C.S. Lee, K.M. Kleinke, H. Kleinke, Solid State Sci. 7 (2005) 1049.
[18] R.H. Mitchell, K.C. Ross, E.G. Potter, J. Solid State Chem. 177 (2004) 1867.
[19] A.M.C. Souza, S.R.O. Neto, C.A. Macedo, J. Magn. Magn. Mater. 272 (2004) 521.
[20] Y.-J. Lu, J.A. Ibers, Comments Inorg. Chem. 14 (1993) 229.
[21] R. Hoppe, E. Vielhaber, Naturwissenschaften 51 (1964) 130.
[22] W. Bronger, H. Balkhardtdegen, D. Schmitz, Z. Anorg. Allg. Chem. 574 (1989) 99.
[23] W. Bronger, O. Gunther, J. Less Common Met. 27 (1972) 73.
[24] W. Bronger, O. Gunther, J. Huster, M. Spangenberg, J. Less Common Met. 50 (1976) 49.
[25] M. Springborg, Chem. Phys. 246 (1999) 347.
[26] K.O. Klepp, Z. Naturforsch., B: Chem. Sci. 47 (1992) 201.
[27] H.D. Rad, R. Hoppe, Z. Naturforsch., B: Chem. Sci. 33 (1978) 1184.
[28] K. Klepp, H. Boller, Monatsh. Chem. 112 (1981) 83.
[29] J. Ensling, P. Gutlich, H. Spiering, K. Klepp, Hyperfine Interact. 28 (1986) 599.
[30] D. Welz, P. Deppe, W. Schaefer, H. Sabrowsky, M. Rosenberg, J. Phys. Chem. Solids 50 (1989) 297.
[31] S.K. Tiwary, S. Vasudevan, Phys. Rev. B 56 (1997) 7812.
[32] D. Welz, M. Nishi, Phys. Rev. B 45 (1992) 9806.
[33] W. Bronger, P. Muller, J. Less Common Met. 70 (1980) 253.
[34] W.M. Reiff, I.E. Grey, A. Fan, Z. Eliezer, H. Steinfink, J. Solid State Chem. 13 (1975) 32.
[35] J.R. Clark, G.E. Brown, Am. Miner. 65 (1980) 477.
[36] M. Reissner, W. Steiner, J. Wernisch, H. Boller, Hyperfine Interact. 169 (2006) 1301.
[37] T. Ohtani, Y. Miyoshi, Y. Fujii, T. Koyakumaru, T. Kusano, K. Minami, Solid State Commun. 120 (2001) 95.
[38] T. Ohtani, S. Onoue, Mater. Res. Bull. 21 (1986) 69.
[39] C.B. Shoemaker, Z. Kristallogr. 137 (1973) 225.
[40] N. Nakayama, K. Kosuge, S. Kachi, T. Shinjo, T. Takada, Abstr. Pap. Am. Chem. Soc. (1979) 58.
[41] I.E. Grey, H. Steinfink, Inorg. Chem. 10 (1971) 691.
[42] T. Baikie, A. Maignan, M.G. Francesconi, Chem. Commun. (2004) 836.
[43] D.A. Headspith, P.D. Battle, M.G. Francesconi, J. Solid State Chem. 180 (2007) 2859.
[44] M.A. Greaney, K.V. Ramanujachary, Z. Teweldemedhin, M. Greenblatt, J. Solid State Chem. 107 (1993) 554.
[45] T. Baikie, V. Hardy, A. Maignan, M.G. Francesconi, Chem. Commun. (2005) 5077.
[46] M.R. Harrison, V. Hardy, A. Maignan, M.G. Francesconi, Chem. Commun. (2009) 2214.
[47] M. Sassmannshausen, H.D. Lutz, Acta Crystallogr., Sect. C 54 (1998) 704.
[48] J.M. Leger, A.M. Redon, C. Andraud, F. Pelle, Phys. Rev. B 41 (1990) 9276.
[49] Z.V. Popovic, G. Mihaly, I. Kezsmarki, H. Berger, L. Forro, V.V. Moshchalkov, Phys. Rev. B (2002) 65.
[50] K. Matsuura, T. Wada, T. Nakamizo, H. Yamauchi, S. Tanaka, Phys. Rev. B 43 (1991) 13118.
[51] R. Itti, T. Wada, K. Matsuura, T. Itoh, K. Ikeda, H. Yamauchi, N. Koshizuka, S. Tanaka, Phys. Rev. B 44 (1991) 2306.
[52] P.C. Donohue, J.F. Weiher, J. Solid State Chem. 10 (1974) 142.
[53] K. Matsuura, T. Wada, N. Suzuki, T. Nakamizo, S. Ikegawa, H. Yamauchi, S. Tanaka, Jpn. J. Appl. Phys., Part 1 29 (1990) L473.
[54] J. Yan, K.V. Ramanujachary, M. Greenblatt, Mater. Res. Bull. 30 (1995) 463.
[55] N. Kijima, K. Morie, S. Chikazawa, H. Nishihara, S. Nagata, J. Solid State Chem. 142 (1999) 57.
[56] B. Okai, K. Takahashi, M. Saeki, J. Yoshimoto, Mater. Res. Bull. 23 (1988) 1575.
[57] J. Peters, B. Krebs, Acta Crystallogr., Sect B: Struct. Sci. 38 (1982) 1270.